7th International Conference on Modelling and Simulation in Nuclear Science and Engineering (7ICMSNSE)
Ottawa Marriott Hotel, Ottawa, Ontario, Canada, October 18-21, 2015

7ICMSNSE-88

Serpent-COREDAX Analysis of CANDU-6 Time-Average Model

Mohammad Abdul Motalab, Bumhee Cho, Woosong Kim, Nam Zin Cho, Yonghee Kim*
Department of Nuclear and Quantum Engineering, KAIST, Daejeon, Korea
yongheekim@kaist.ac.kr

Abstract

COREDAX-2 is the nuclear core analysis nodal code that has adopted the Analytic Function Expansion Nodal (AFEN) methodology which has been developed in Korea. AFEN method outperforms in terms of accuracy compared to other conventional nodal methods. To evaluate the possibility of CANDU-type core analysis using the COREDAX-2, the time-average analysis code system was developed. The two-group homogenized cross-sections were calculated using Monte Carlo code, Serpent2. A stand-alone time-average module was developed to determine the time-average burnup distribution in the core for a given fuel management strategy. The coupled Serpent-COREDAX-2 calculation converges to an equilibrium time-average model for the CANDU-6 core.

Keywords: COREDAX-2, AFEN, CANDU-6, Time-average core, Serpent2.

1. Introduction

The CANDU-6 (CANada Deuterium Uranium) reactor is a heavy water cooled reactor, four of which are being operated in Korea. Currently, the core calculation of the CANDU-6 totally relies on the Canadian AECL's coarse-mesh FDM code, RFSP [1]. However, the RFSP code is found to be subject to inconsistency issue mainly due to the lack of nodal equivalence [2]. Therefore, lattice calculation and 3-dimensional core analysis code system should be built to improve the reliability of CANDU-6 core analysis.

Because of the on-line refuelling of CANDU-6 reactor during operation, the time-average model is often used to obtain the equilibrium core which neglect the daily variations [3]. In this study, the time-average model calculation of CANDU-6 reactor was performed by using the Analytic Function Expansion Nodal (AFEN) method based nodal code, COREDAX-2 [4]. Although the COREDAX was originally developed for the LWR core analysis, it was shown in the previous study that it can be used for the CANDU-6 core analysis if the appropriate core model is used. To generate 2-group cross-section data for COREDAX-2, the Monte Carlo method based lattice code, Serpent 2 [5] was used.

2. Analytic Function Expansion Nodal (AFEN) Method

In this section, the AFEN method used in COREDAX-2 code is introduced [4]. The AFEN method in steady-state starts from the multigroup steady-state diffusion equation for a homogenized cuboid node *m* with side length of h_x^m, h_y^m, h_z^m which can be written in matrix form as follows:

$$-\nabla \cdot \left[D^m\right]\nabla \vec{\phi}^m(\vec{r}) + \left[A^m\right]\vec{\phi}^m(\vec{r}) = \frac{1}{k_{eff}} \vec{\chi}_0^m \left[F^m\right]^T \vec{\phi}^m(\vec{r}), \tag{1}$$

where,

$$\left[D^m\right] = \begin{pmatrix} D_1^m & & \\ & \ddots & \\ & & D_G^m \end{pmatrix},$$

$$\left[A^m\right] = \begin{pmatrix} \Sigma_{r1}^m & -\Sigma_{s2\to1}^m & \cdots & -\Sigma_{sG\to1}^m \\ -\Sigma_{s1\to2}^m & \Sigma_{r2}^m & \cdots & -\Sigma_{sG\to2}^m \\ \vdots & \vdots & \ddots & \vdots \\ -\Sigma_{s1\to G}^m & -\Sigma_{s2\to G}^m & \cdots & \Sigma_{rG}^m \end{pmatrix},$$

$$\left[F^m\right]^T = \left[\nu\Sigma_{f1}^m \cdots \nu\Sigma_{fG}^m\right],$$

and

m	:	node index,
G	:	maximum group number,
D_g^m	:	diffusion coefficient of group *g*,
Σ_{rg}^m	:	removal cross section of group *g*,
$\Sigma_{sg\to g'}^m$	:	scattering cross section from group *g* to *g'*,
Σ_{fg}^m	:	fission cross section of group *g*,
ν	:	average number of neutrons released per fission,
$\vec{\chi}_0$	:	prompt neutron fission spectrum vector.

All the quantities are defined within a homogenized node. In contrast to the most modern nodal methods that solve the transverse-integrated equivalent one-dimensional diffusion equations, AFEN directly solves the original diffusion equations. The flux distribution within a node is expanded into the subset of analytic solutions as follows:

$$\vec{\phi}(x,y,z) = \vec{E} + \vec{\varphi}(x,y,z) + \vec{\varphi}(y,x,z) + \vec{\varphi}(z,x,y), \tag{2}$$

where

$$\begin{aligned}\vec{\varphi}(x,y,z) = \sinh\left(\sqrt{\Lambda^m}x\right)\left(\vec{A}_0^x + y\vec{A}_1^x + z\vec{A}_2^x\right) \\ + \cosh\left(\sqrt{\Lambda^m}x\right)\left(\vec{B}_0^x + y\vec{B}_1^x + z\vec{B}_2^x\right),\end{aligned} \tag{3}$$

$$\left[\Lambda^m\right] = \left[D^m\right]^{-1}\left(\left[A^m\right] - \frac{\vec{\chi}_0}{k_{eff}}\left[F^m\right]^T\right). \tag{4}$$

In the early stages of power iterations, the exact multiplication factor is not known. To circumvent this issue, a constant term in the flux expansion, $\vec{E}$ is introduced. Therefore, the number of known coefficient vector is nineteen per node. Before the unknown coefficient vectors are expressed in terms of known variables explicitly, the matrix functions such as $\sinh\left(\sqrt{\Lambda^m}x\right)$ and $\cosh\left(\sqrt{\Lambda^m}x\right)$ should be evaluated. One such matrix functions are treated like normal variables, then the unknown coefficient vectors are expressed in terms of nineteen nodal unknowns with matrix function coefficients. The corresponding nineteen nodal unknowns are a node-average flux, six interface fluxes, and twelve interface flux moments defined as follows:

$$\left[\bar{\phi}^m\right] = \frac{1}{h_x^m h_y^m h_z^m}\int_{-h_z^m/2}^{h_z^m/2}\int_{-h_y^m/2}^{h_y^m/2}\int_{-h_x^m/2}^{h_x^m/2}\vec{\phi}^m(x,y,z)dxdydz, \tag{5}$$

$$\left[\tilde{\phi}^m\right] = \frac{1}{h_y^m h_z^m}\int_{-h_z^m/2}^{h_z^m/2}\int_{-h_y^m/2}^{h_y^m/2}\vec{\phi}^m\left(-\frac{h_x^m}{2},y,z\right)dydz, \tag{6}$$

$$\left[\tilde{\psi}_{x0}^{m1}\right] = \frac{1}{h_y^m h_z^m}\int_{-h_z^m/2}^{h_z^m/2}\int_{-h_y^m/2}^{h_y^m/2} w_1(y,z)\vec{\phi}^m\left(-\frac{h_x^m}{2},y,z\right)dydz, \tag{7}$$

$$\left[\tilde{\psi}_{x0}^{m2}\right] = \frac{1}{h_y^m h_z^m}\int_{-h_z^m/2}^{h_z^m/2}\int_{-h_y^m/2}^{h_y^m/2} w_2(y,z)\vec{\phi}^m\left(-\frac{h_x^m}{2},y,z\right)dydz, \tag{8}$$

where the weighting functions are

$$w_1(y,z) = \frac{2y}{h_y}, \qquad w_2(y,z) = \frac{2z}{h_z}.$$

And same procedure is applied to other interface surfaces.

The subscripts on the nodal quantities refer to the interface of the node as in Figure 1.

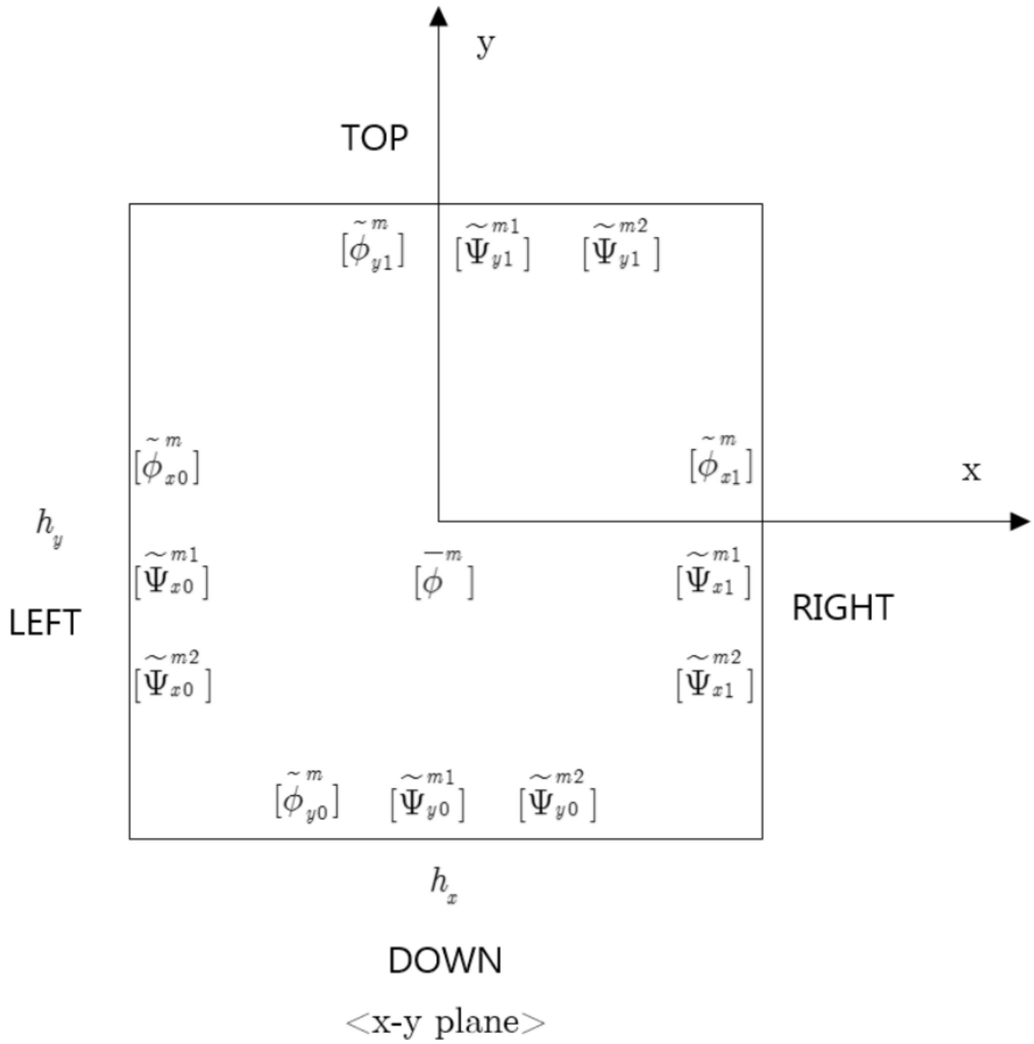

Figure 1. Geometry of node *m*.

For 19 coefficients with 19 nodal quantities, 19 equations are required to update 19 nodal quantities. Those 19 equations include a node balance equation, 6 interface current continuity equations and 12 interface current moment continuity equations. By solving 19 equations, nodal quantities are updated and k_{eff} value is evaluated from the power method.

3. Two-group Homogenized Parameter Generation

To generate the two-group homogenized parameters for the COREDAX-2 input, a detailed 3-dimensional fuel lattice was modelled including 'end cap' as shown in Figure 2 and Table 1. The lattice calculation was performed using DBRC method implemented Monte Carlo code, Serpent 2. For the nuclear data library, ENDF/B-VII.0 was used. The depletion calculation was performed for 240 days with 0.34034 MWth power.

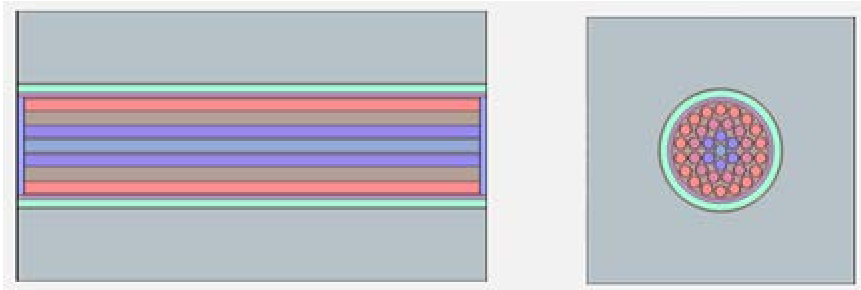

Figure 2. CANDU-6 standard lattice configuration

Parameters	Value
Geometric Parameters	
Fuel radius	0.6077 cm
Cladding outer radius	0.64808 cm
Lattice pitch	28.575 cm
Calandria tube outer radius	6.58954 cm
Calandria tube inner radius	6.44988 cm
CO_2 gap thickness	0.83722 cm
Pressure tube outer radius	5.61266 cm
Pressure tube inner radius	5.17915 cm
Thermal parameters	
Fuel Temperature	960.16 K
Coolant Temperature	561.16 K
Coolant Density	0.81493 g/cm3
Moderator Temperature	342.16 K
Moderator Density	1.085089 g/cm3

Table 1. CANDU-6 equivalent core lattice design parameters

In CANDU-6 core, reactivity devices such as Liquid Zone Controller (LZC), Mechanical Controller Absorber (MCA), Shutoff Rod (SOR), and Adjuster Rods are vertically inserted. Therefore, incremental cross sections are evaluated by using 3-dimensional lattice calculation to consider reactivity devices for 2-group homogenized parameters. The incremental cross section is defined as the difference of cross sections between the reactivity devices inserted supercell lattice and standard lattice. Every supercell lattices are modelled for the 3-dimensional Monte Carlo code, Serpent 2 as shown in Figure 3 and its incremental cross section as shown in Table 2.

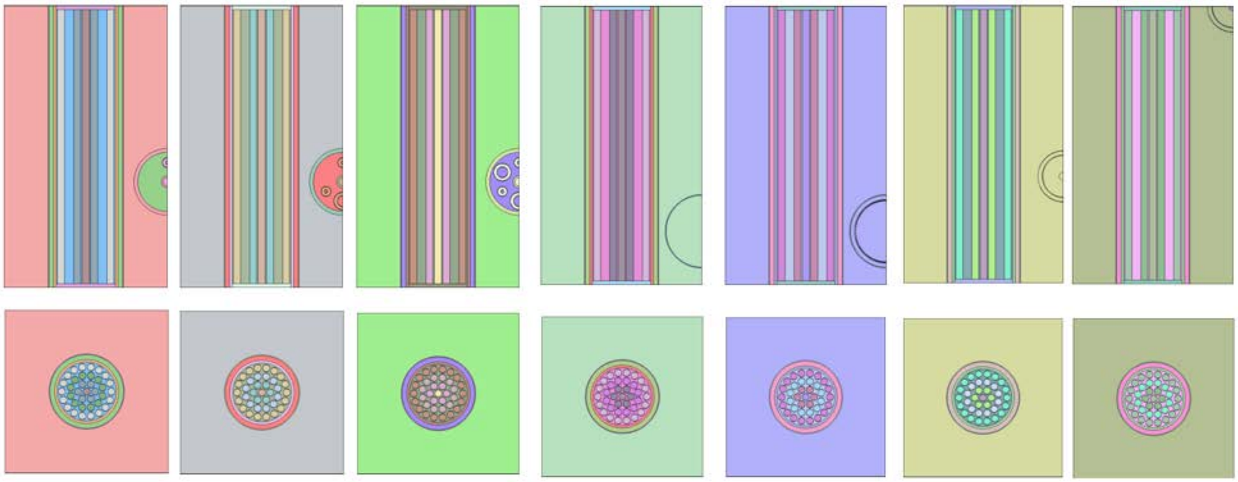

Figure 3. Supercell lattice with different LZC, MCA, and adjuster rods

Incremental cross section (cm^{-1})	$\Delta\Sigma_{tr,1}$	$\Delta\Sigma_{tr,2}$	$\Delta\Sigma_{a,1}$	$\Delta\Sigma_{a,2}$	$\Delta\nu\Sigma_{f,1}$	$\Delta\nu\Sigma_{f,2}$	$\Delta\Sigma_{s,1\to2}$
LZC2, Empty	-7.53E-03	-1.27E-02	-1.03E-05	3.21E-05	-1.52E-05	1.41E-05	-2.99E-04
LZC4, Empty	-5.94E-03	-6.88E-03	-3.07E-06	8.34E-05	-7.98E-06	1.28E-05	-1.20E-04
LZC6, Empty	-4.41E-03	-6.41E-04	3.16E-06	1.38E-04	-1.76E-06	1.04E-05	4.92E-05
LZC2, Full	1.76E-03	5.36E-02	3.49E-05	5.84E-04	2.24E-05	1.24E-05	8.22E-04
LZC4, Full	1.67E-03	5.12E-02	3.45E-05	5.67E-04	2.21E-05	1.05E-05	8.04E-04
LZC6, Full	1.48E-03	4.75E-02	3.35E-05	5.38E-04	2.15E-05	8.06E-06	7.72E-04
ADJ-D	3.61E-04	1.91E-04	1.08E-05	1.99E-04	-2.55E-06	1.33E-05	5.14E-05
ADJ-C, Inner	5.40E-04	2.97E-04	1.50E-05	2.54E-04	-3.27E-06	1.90E-05	6.36E-05
ADJ-C, Outer	6.65E-04	3.92E-04	1.89E-05	3.29E-04	-4.40E-06	2.27E-05	8.46E-05
ADJ-B	8.79E-04	5.08E-04	2.38E-05	3.90E-04	-5.18E-06	2.75E-05	9.86E-05
MCA, Empty	8.29E-05	-2.76E-04	2.96E-06	1.40E-05	-9.10E-07	1.06E-06	-1.48E-05
ADJ-A, Inner	3.93E-04	2.07E-04	1.12E-05	2.10E-04	-2.75E-06	1.45E-05	5.44E-05
ADJ-A, Outer	5.31E-04	2.99E-04	1.53E-05	2.70E-04	-3.60E-06	1.87E-05	6.98E-05
ADJ-C, Inner Quarter	2.94E-04	1.52E-04	7.04E-06	1.25E-04	-1.44E-06	1.06E-05	2.98E-05
ADJ-C, Outer Quarter	3.29E-04	2.00E-04	9.06E-06	1.60E-04	-1.75E-06	1.29E-05	4.04E-05
ADJ-B Quarter	4.28E-04	2.61E-04	1.18E-05	1.88E-04	-2.11E-06	1.49E-05	4.69E-05
ADJ-A, Inner Quarter	1.96E-04	1.10E-04	5.50E-06	1.04E-04	-1.21E-06	8.35E-06	2.64E-05
ADJ-A, Outer Quarter	2.71E-04	1.55E-04	7.28E-06	1.33E-04	-1.67E-06	1.08E-05	3.49E-05
ADJ-D Quarter	3.65E-04	-1.19E-04	1.18E-05	1.52E-04	-2.56E-06	1.18E-05	1.89E-05

Table 2. Incremental cross sections

4. Time-Average Model

In order to use COREDAX-2 code for the CANDU-6 core analysis, time-average model was considered for the equilibrium-core simulation [3]. The time-average model of CANDU-6 core is not an average over time of core snapshots, but a model in which lattice cross sections at each bundle location averaged over residence time of fuel at that location. The time-average cross section at the channel number *j* and the axial position *k* is defined as follows:

$$\Sigma_{i,jk}(t.av.) = \frac{\frac{1}{T_j}\int_0^{T_j} \Sigma_i(\omega(t))\hat{\phi}_{jk}\,dt}{\frac{1}{T_j}\int_0^{T_j} \hat{\phi}_{jk}\,dt}, \quad (9)$$

where

ω : fuel irradiation,
$\Sigma_{i,jk}$: a particular cross section Σ_i at position *jk*,
T_j : the average time between refuellings of channel *j*,
$\hat{\phi}_{jk}$: the Westcott flux in fuel at position *jk*.

In Equation (9), the cross section according to fuel irradiation was evaluated from the cross section according to the burnup by using below linear relationship between irradiation and burnup.

$$\omega(n/kbarn) = 0.35275 \times Burnup(GWd/tU) \quad (10)$$

And Equation (9) can be rewritten as Equation (11) using $d\omega = \hat{\phi}dt$.

$$\Sigma_{i,jk}(t.av.) = \frac{1}{\omega_{out,jk} - \omega_{in,jk}} \int_{\omega_{in,jk}}^{\omega_{out,jk}} \Sigma_i(\omega)d\omega, \quad (11)$$

where $\omega_{in,jk}$ and $\omega_{out,jk}$ are the in-coming and out-going fuel irradiation at position *jk*, respectably. For the *N*-bundle-shift push-through refuelling scheme (total 12 bundle per channel), the incoming and outgoing irradiation are derived as follows:

$$\omega_{out,jk} = \omega_{in,jk} + \hat{\phi}_{jk} \cdot T_j, \quad (12)$$

$$\omega_{in,jk} = \begin{cases} 0 & for\ 1 \le k \le N, \\ \omega_{out,j(k-N)} & for\ N < k \le 12. \end{cases} \quad (13)$$

Also, the exit irradiation in channel *j* is defined as the average of outgoing irradiation over the *N* bundles leaving the channel at each refuelling:

$$\omega_{exit,j} = \frac{1}{N}\sum_{k=13-N}^{12}\omega_{out,jk} = \frac{1}{N}\sum_{k=1}^{12}\hat{\phi}_{jk}T_j = \frac{T_j}{N}\sum_{k=1}^{12}\hat{\phi}_{jk}. \quad (14)$$

From Equation (14), the channel dwell times T_j is obtained as below:

$$T_j = \frac{N \cdot \omega_{exit,j}}{\sum_{k=1}^{12} \hat{\phi}_{jk}}. \tag{15}$$

Therefore, the time-average model of CANDU-6 core can be obtained by using Equations (11), (12), (13), and (15) with neutron diffusion equation. This equation set must be solved iteratively until cross-consistency is attained.

In this study, neutron diffusion equation was solved using COREDAX-2 code and independent time-average module was developed to calculate the time-average cross sections. The time-average module and COREDAX-2 code are coupled by Windows batch script. During iteration, the time-average module use COREDAX-2 flux distribution output to generate time-average cross sections and prints out them in the COREDAX-2 input format so that COREDAX-2 can solve neutron diffusion equation using given time-average cross section. The flowchart of time-average iteration calculation is shown is Figure 4.

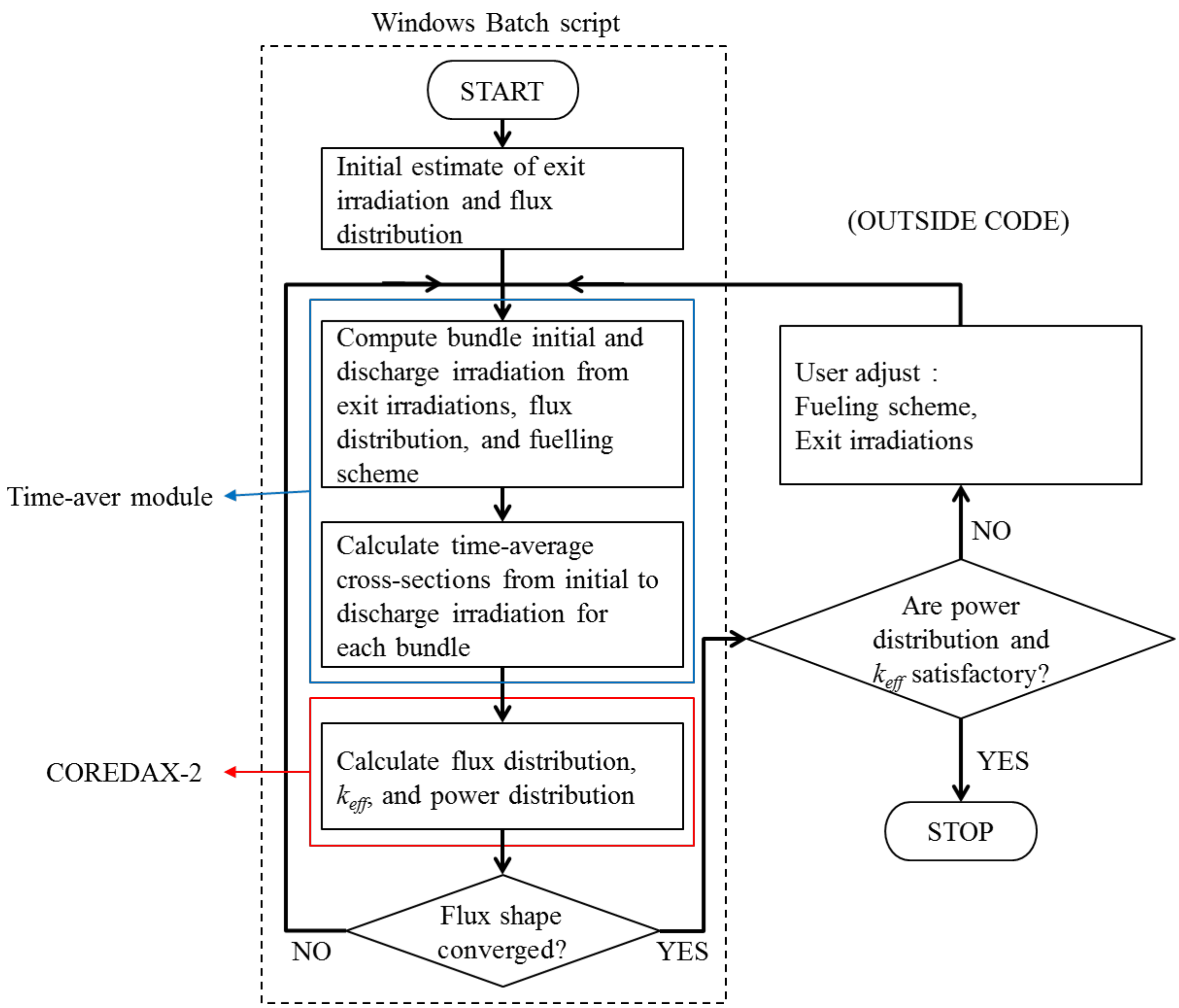

Figure 4. The flowchart of time-average iteration calculation using COREDAX-2

5. Time-Average Core Analysis Results

The CANDU time-average core analysis code using COREDAX-2 was tested using general CANDU-6 core model. It is assumed that all adjuster rods are fully inserted and the LZCs keep 50 % water level during normal operation. Also, as the time-average model input, the 8-bundle-shifting was assumed and zone-wise exit irradiation shown in Figure 5 is used. The time-average iteration is assumed to be converged when the maximum relative flux difference between iteration steps are smaller than 0.1%.

After 12 iteration steps, the final effective multiplication factor value was k_{eff} = 0.9979780, which was very close to the critical. After the time-average calculation, the 14 zone-wise power distribution of CANDU reactor is printed out to check whether it satisfies the target power distribution or not. The k_{eff} results and zone power are shown in Table 3 and 4.

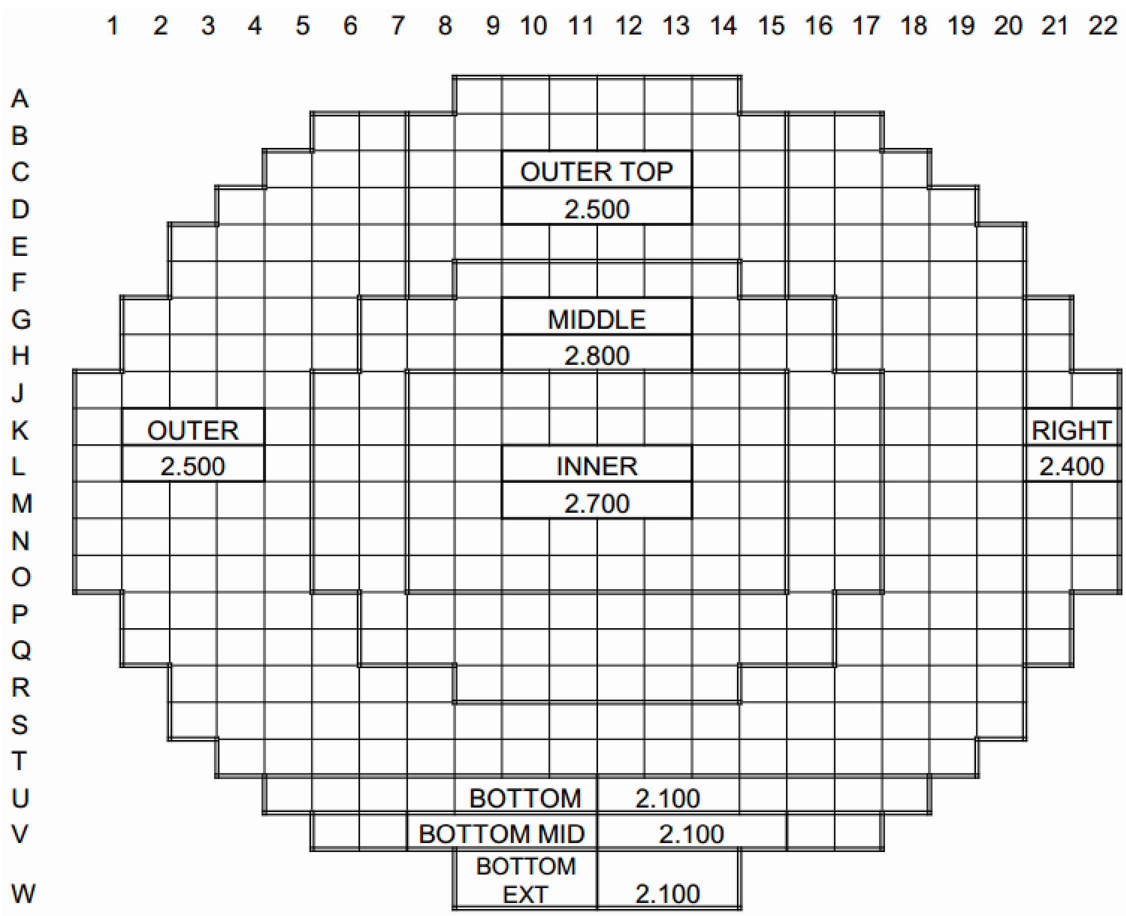

Figure 5. Zone-wise exit irradiation for time-average calculation input.

iteration step	k_{eff}	maximum flux relative error
0	0.9981353	-
1	0.9980119	3.45%
2	0.9979617	1.49%
3	0.9979817	0.75%
4	0.9979745	0.41%
5	0.9979764	0.28%
6	0.9979762	0.20%
7	0.9979756	0.17%
8	0.9979767	0.17%
9	0.9979769	0.13%
10	0.9979764	0.12%
11	0.9979757	0.11%
12	0.9979780	0.10%

Table 3. The k_{eff} value for each time-average iteration steps.

Zone	Power (MWth)	Zone	Power (MWth)
1	125.543	8	125.382
2	130.710	9	130.776
3	166.800	10	166.776
4	164.829	11	164.802
5	183.779	12	183.752
6	126.843	13	126.967
7	132.273	14	132.166

Table 4. Zone power result of final time-average core model.

The channel power distribution channel dwell time and channel average discharge burnup are obtained as time-average calculation and they are shown in Figure 6, 7 and 8. The core average discharge burnup about 7.23 GWth/MTU is achieved in this time-average calculation.

	1	2	3	4	5	6	7	8	9	10	11	12	13	14	15	16	17	18	19	20	21	22
A									2680	2865	2969	2968	2865	2683								
B						2412	2988	3494	3778	3967	4037	4038	3970	3784	3502	2996	2421					
C					2753	3382	4006	4503	4835	4992	5002	5006	5001	4846	4515	4018	3396	2771				
D				2838	3580	4312	4930	5380	5657	5756	5720	5727	5768	5672	5398	4949	4332	3606	2865			
E			2688	3548	4370	5053	5575	5932	6132	6185	6132	6140	6201	6152	5955	5599	5082	4404	3585	2720		
F			3375	4241	4994	5553	5924	6168	6246	6277	6251	6259	6295	6269	6196	5956	5592	5038	4288	3420		
G		2965	3947	4823	5444	5880	6115	6287	6368	6404	6424	6432	6425	6395	6320	6155	5928	5497	4881	4005	3025	
H		3492	4485	5305	5809	6149	6333	6469	6522	6552	6585	6593	6573	6552	6507	6379	6205	5870	5373	4557	3569	
J	2771	3889	4938	5689	6093	6322	6542	6680	6693	6689	6702	6709	6710	6724	6721	6594	6384	6162	5767	5024	3982	2845
K	3043	4211	5272	5979	6309	6494	6717	6840	6815	6760	6713	6719	6779	6846	6882	6771	6559	6383	6066	5368	4316	3128
L	3220	4405	5475	6190	6529	6694	6870	6958	6903	6814	6733	6737	6831	6933	7000	6925	6761	6609	6281	5576	4517	3312
M	3238	4436	5527	6274	6647	6814	6963	7027	6961	6867	6784	6788	6883	6990	7069	7018	6881	6728	6367	5629	4548	3331
N	3092	4294	5410	6205	6636	6829	6971	7033	6981	6917	6868	6872	6932	7009	7074	7024	6895	6715	6295	5508	4401	3178
O	2838	4001	5117	5968	6487	6732	6875	6958	6948	6940	6954	6958	6955	6975	6996	6925	6794	6560	6050	5205	4095	2913
P		3605	4654	5544	6117	6489	6661	6790	6845	6883	6922	6927	6898	6870	6825	6706	6544	6181	5616	4728	3684	
Q		3061	4080	4988	5635	6117	6412	6636	6752	6811	6839	6843	6824	6775	6667	6452	6164	5689	5046	4139	3121	
R			3471	4339	5085	5708	6211	6561	6701	6766	6748	6752	6778	6721	6589	6245	5748	5129	4384	3514		
S			2761	3628	4457	5226	5904	6394	6682	6780	6735	6739	6791	6700	6419	5934	5258	4491	3661	2790		
T				2943	3748	4586	5340	5920	6295	6450	6428	6432	6460	6310	5940	5364	4611	3773	2966			
U					2990	3739	4496	5125	5568	5797	5835	5838	5805	5581	5141	4514	3758	3008				
V						2717	3421	4059	4444	4715	4834	4836	4720	4453	4071	3434	2730					
W									3192	3451	3606	3608	3455	3198								

Figure 6. Channel power distribution (kWth)

	1	2	3	4	5	6	7	8	9	10	11	12	13	14	15	16	17	18	19	20	21	22
A									399	377	364	364	377	399								
B						444	361	309	288	275	271	270	275	288	309	360	443					
C					390	322	273	242	226	219	218	218	218	225	242	272	321	388				
D				378	304	253	222	203	193	190	191	191	189	193	202	221	252	302	374			
E			398	307	250	216	196	184	178	177	178	178	176	178	183	195	215	248	304	394		
F			320	257	219	197	185	177	195	195	195	195	194	195	177	184	195	217	255	316		
G		361	276	226	201	186	200	194	192	191	190	190	190	191	193	198	184	199	224	272	340	
H		310	243	206	188	178	193	189	187	186	185	185	186	186	188	191	176	186	203	240	291	
J	386	280	221	192	179	193	186	176	176	176	176	176	176	175	175	185	191	177	189	217	263	362
K	355	259	207	183	173	188	182	172	173	174	175	175	174	172	171	180	186	171	180	203	243	331
L	335	248	199	176	168	182	178	169	171	173	175	175	172	170	168	176	181	166	174	196	232	313
M	333	246	198	174	165	179	175	168	169	172	174	173	171	169	167	174	177	163	172	194	231	311
N	349	254	202	176	165	179	175	167	169	170	171	171	170	168	166	174	177	163	173	198	238	326
O	377	272	213	183	168	181	177	169	170	170	169	169	169	169	168	176	180	167	180	210	256	353
P		300	235	197	179	168	183	180	178	177	176	176	177	178	179	182	167	177	194	231	282	
Q		350	267	219	194	179	190	184	181	179	179	178	179	180	183	189	177	192	216	263	329	
R			311	252	215	191	176	167	182	180	181	181	180	182	166	175	190	213	249	307		
S			387	300	245	209	185	171	163	161	162	162	161	163	170	184	208	243	297	383		
T				364	291	238	204	184	173	169	170	170	169	173	184	204	237	289	361			
U					302	245	205	179	165	159	158	158	158	165	179	204	244	300				
V						332	266	224	206	195	190	190	195	206	224	265	331					
W									282	263	252	252	263	282								

Figure 7. Channel dwell time (days)

	1	2	3	4	5	6	7	8	9	10	11	12	13	14	15	16	17	18	19	20	21	22
A									7.01	7.06	7.07	7.07	7.06	7.00								
B						7.01	7.06	7.07	7.13	7.15	7.15	7.15	7.14	7.13	7.07	7.06	7.01					
C					7.03	7.13	7.15	7.15	7.15	7.15	7.15	7.15	7.15	7.15	7.15	7.15	7.13	7.03				
D				7.02	7.13	7.15	7.15	7.15	7.15	7.15	7.15	7.15	7.15	7.15	7.15	7.15	7.15	7.14	7.02			
E			7.01	7.13	7.15	7.15	7.15	7.15	7.15	7.15	7.15	7.15	7.15	7.15	7.15	7.15	7.15	7.15	7.13	7.01		
F			7.07	7.15	7.15	7.15	7.16	7.16	7.99	7.99	7.99	7.99	7.99	7.99	7.16	7.16	7.15	7.15	7.15	7.07		
G		7.00	7.13	7.15	7.15	7.15	7.99	7.99	7.99	7.99	7.99	7.99	7.99	7.99	7.99	7.99	7.15	7.15	7.15	7.13	6.73	
H		7.08	7.15	7.15	7.15	7.15	7.99	7.99	7.99	7.99	7.99	7.99	7.99	7.99	7.99	7.99	7.15	7.15	7.15	7.15	6.80	
J	7.01	7.13	7.15	7.15	7.15	7.98	7.99	7.71	7.71	7.71	7.71	7.71	7.71	7.71	7.71	7.99	7.98	7.15	7.15	7.15	6.85	6.73
K	7.06	7.15	7.15	7.15	7.16	7.99	7.99	7.71	7.71	7.71	7.71	7.71	7.71	7.71	7.71	7.98	7.99	7.16	7.15	7.15	6.87	6.79
L	7.07	7.15	7.15	7.15	7.16	7.99	7.99	7.71	7.71	7.71	7.71	7.71	7.71	7.71	7.71	7.99	7.99	7.16	7.15	7.15	6.87	6.79
M	7.06	7.15	7.15	7.15	7.16	7.99	7.98	7.71	7.71	7.71	7.71	7.71	7.71	7.71	7.71	7.98	7.99	7.16	7.15	7.15	6.87	6.79
N	7.07	7.14	7.15	7.15	7.16	7.99	7.99	7.71	7.71	7.71	7.71	7.71	7.71	7.71	7.71	7.99	7.99	7.16	7.15	7.15	6.87	6.79
O	7.00	7.13	7.15	7.15	7.15	7.98	7.99	7.71	7.71	7.71	7.71	7.71	7.71	7.71	7.71	7.99	7.98	7.15	7.15	7.15	6.85	6.73
P		7.07	7.15	7.15	7.15	7.15	7.99	7.99	7.99	7.99	7.99	7.99	7.99	7.99	7.99	7.99	7.15	7.15	7.15	7.15	6.79	
Q		7.01	7.13	7.15	7.15	7.15	7.99	7.99	7.99	7.99	7.99	7.99	7.99	7.99	7.99	7.99	7.15	7.15	7.15	7.13	6.73	
R			7.07	7.14	7.15	7.15	7.16	7.16	7.99	7.99	7.99	7.99	7.99	7.99	7.16	7.16	7.15	7.15	7.14	7.07		
S			7.00	7.13	7.15	7.15	7.15	7.15	7.15	7.15	7.15	7.15	7.15	7.15	7.15	7.15	7.15	7.15	7.13	7.00		
T				7.02	7.13	7.15	7.15	7.15	7.15	7.15	7.15	7.15	7.15	7.15	7.15	7.15	7.15	7.13	7.02			
U					5.91	6.01	6.02	6.02	6.02	6.02	6.03	6.03	6.02	6.02	6.02	6.02	6.01	5.91				
V						5.91	5.95	5.96	6.01	6.02	6.02	6.02	6.02	6.00	5.96	5.95	5.91					
W									5.90	5.95	5.95	5.95	5.95	5.90								

Figure 8. Channel average discharge burnup (GWth/TU)

6. Conclusion

In this study, CANDU6 time-average calculation was performed by using Serpent 2 and COREDAX-2. The final time-average model provided near critical k_{eff} value and flat power distribution. However, there was non-negligible discrepancy between our result and RFSP-IST result. It is mainly because the COREDAX-2 code is nodal code based on the Analytic Function Expansion Nodal (AFEN) method, which is much more accurate than the coarse mesh Finite Difference Method (FDM) of RFSP-IST code. It is also expected that Serpent 2 lattice calculation based on the Monte Carlo method will provide much more accurate 2-group homogenized parameters than the conventional WIMS/DRAGON lattice calculation. More detailed code validation and CANDU-6 analysis are still remains for the future task.

7. References

[1] W. Shen and B. Phelps, "Assessment of the Coarse-Mesh Finite-Difference Method with the Multicell Methodology in RFSP for ACR-1000," Proceedings of 30th CNS Annual Conference, Calgary, June, 2009

[2] Y. Kim, W. Kim, D. Hartanto, and B.H. Cho, "Effectiveness of the Nodal Equivalence Theory in CANDU Reactor," Transactions of the American Nuclear Society vol. 107, San Diego, CA, USA, November 11-15, 2012

[3] W. Shen, "RFSP-IST Version REL_3-04 Theory Manual", COG Report SQAD-06-5058 / AECL Report 153-117360-STM-002, 2006 December.

[4] B. Cho and N.Z. Cho, "Theory Manual for the Rectangular Three-Dimensional Diffusion Nodal Code COREDAX-2 Version 1.0," KINS/HR-1356, NURAPT-2014-02, KAIST/KINS, August 2014

[5] J. Leppanen. "PSG2 / Serpent - a Continuous-energy Monte Carlo Reactor Physics Burnup Calculation Code," VTT Technical Research Centre of Finland, Jun. 13, 2012